

1 The High-Luminosity LHC and Phase-2 of CMS

1.1 High-Luminosity LHC and CMS

In order to sustain and extend the LHC's physics discovery program and maintain operability for a decade or more, the LHC is undergoing a major upgrade to the High-Luminosity LHC (HL-LHC). In its final configuration, the HL-LHC will deliver a peak luminosity of $7.5 \times 10^{34} \text{ cm}^{-2} \text{ s}^{-1}$, potentially leading to total integrated luminosity of 4000 fb^{-1} after ten years of operations, scheduled to begin in 2027 [CITE]. This integrated luminosity is about ten times the predicted luminosity reach of the LHC in its initial configuration. To maximize the discovery potential of this unprecedented amount of data, the CMS detector is undergoing Phase-2 upgrades in order to perform high-precision measurements and searches for physics beyond the Standard Model in the intense running conditions of the HL-LHC.

1.2 The Phase-2 Level-1 Trigger

To achieve the goals of the HL-LHC program and to ensure the collection of information-rich datasets in the HL-LHC, the Phase-2 upgrade of the CMS Level-1 Trigger must be upgraded in conjunction with the CMS sub-detectors and their readouts, to maintain physics selectivity. The HL-LHC will produce an intense hadronic environment corresponding to 200 simultaneous collisions per beam crossing, necessitating comprehensive upgrades of the trigger system outlined below.

To profit from the extended coverage and increased granularity of the upgraded CMS detector, the latency of the L1 trigger system (time available to produce a L1 Accept signal) will be increased significantly from $3.8 \mu\text{s}$ to $12.5 \mu\text{s}$, with an increased maximum output bandwidth of 750 kHz. [CITE]. With the increased latency, in addition to information from calorimeters and muon detectors (as in the Phase-1 system), information from the new tracker and high-granularity endcap calorimeter can also be included at L1 for the first time. This is illustrated in the functional diagram of the architecture of the Phase-2 trigger system in Fig. 1.

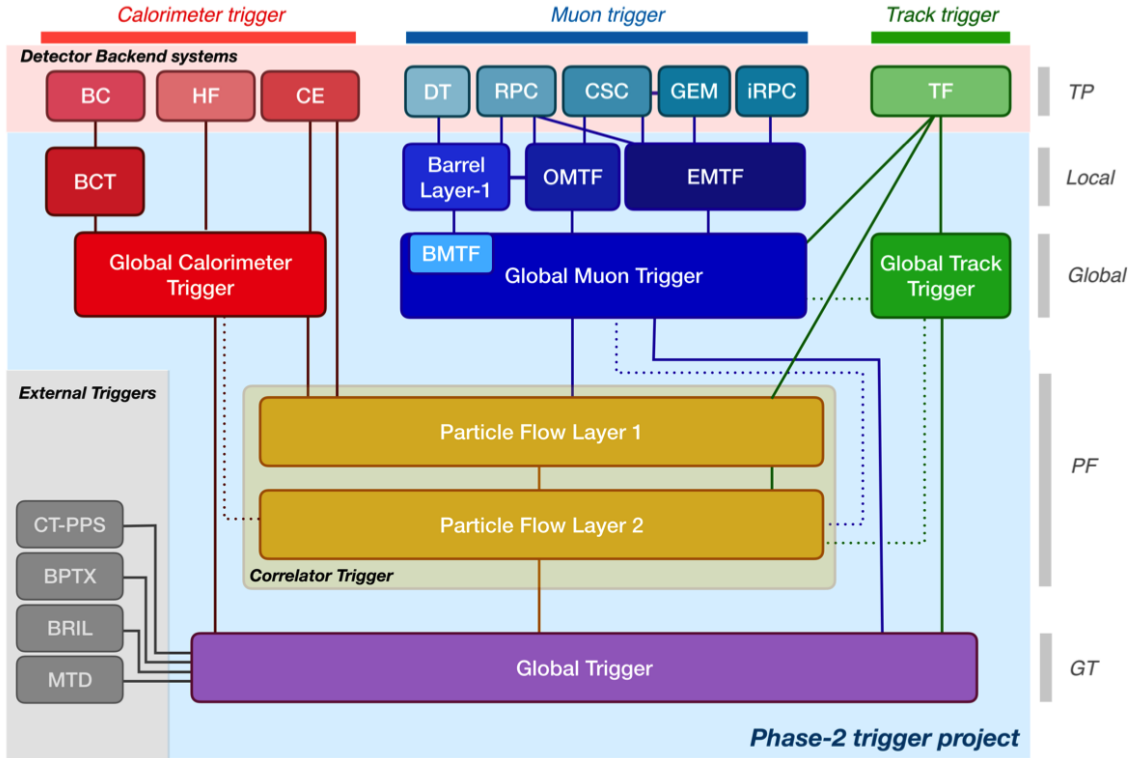


Figure 1: Functional diagram of the CMS L1 Phase-2 upgraded trigger design from [CITE] <https://cds.cern.ch/record/2714892/files/CMS-TDR-021.pdf>, showing the four trigger paths: calorimeter, muon, track, and Particle Flow. For the first time, tracking information will be available as early as the L1 Trigger.

The key feature of the Phase-2 L1 Trigger is the introduction of a correlator layer, where algorithms produce higher-level trigger objects by combining information from sub-detectors, with a selectivity approaching that of offline reconstruction in the HLT. Four independent data processing paths (grouped together in Fig. 1) are implemented: tracking, calorimetry, muon systems, and particle-flow techniques:

- **Calorimeter Trigger path:** (*red*, Fig. 1) A barrel calorimeter trigger (BCT) and the HGCALE backend are used to produce high-granularity information from the calorimeters to produce high-resolution clusters and identification variables used for later processing. Outputs from the BCT, HGCALE, and the HF are sent to a global calorimeter trigger (GCT), where calorimeter-only objects such as e/γ candidates, hadronically decaying tau lepton candidates, jets, and energy sums are built.
- **Track Trigger path:** (*green*, Fig. 1) Tracks from the Outer Tracker are reconstructed in the track finder (TF) processors as part of the detector backend. A global track trigger (GTT) will reconstruct the primary vertices of the event, along with tracker-only based objects, such as jets and missing transverse momentum.
- **Muon Trigger path:** (*blue*, Fig. 1) Trigger primitives are processed by muon track finder algorithms, again separated into the barrel (barrel muon track finder, BMTF), overlap (overlap muon track finder, OMTF), and endcap (endcap muon track finder, EMTF). Standalone muons and stubs containing information such as position, bend angle, and timing, as well as L1 tracks, are sent to the global muon trigger (GMT).
- **Particle-Flow Trigger path:** (*yellow*, Fig. 1) The correlator trigger (CT) aims to approach the performance of offline Particle Flow, and is implemented in two layers. “Layer-1” produces the particle-flow candidates from matching calorimeter clusters and tracks. “Layer 2” builds and sorts final trigger objects and applies additional identification and isolation criteria.

The outputs from the above trigger paths are combined in the Global Trigger (GT) (*purple*, Fig. 1), which calculates the final trigger decision (Level-1 Accept), transmitting it to the Trigger Control and Distribution System (TCDS), which distributes it to the detector backend systems, initiating the readout to the DAQ. The GT also provides the interface to external triggers (*grey*, Fig. 1), such as triggers for the precision proton spectrometer (PPS), beam position and timing monitors (BPTX), and luminosity and beam monitoring (BRIL) detectors. The design of the Phase-2 Level-1 Trigger allows for future inclusion of triggering information, for instance information about minimum ionizing particles (MIPs) from the MIP Timing Detector (MTD).

1.3 Standalone Barrel Calorimeter electron/photon reconstruction

The reconstruction and identification of electrons and photons (e/γ) begin with the trigger primitives of the barrel ECAL and HCAL detectors and endcap HGCALE calorimeters, covering the pseudorapidity region $|\eta| < 3$. The barrel and endcap regions of the detector are intrinsically different enough to warrant different approaches to e/γ reconstruction. This work focuses on the Standalone Calorimeter e/γ reconstruction taking place in the barrel (Fig. 2).

1.3.1 Phase-2 geometry of the ECAL Barrel trigger

In Phase-2, the upgrade of both on-detector and off-detector electronics for the barrel calorimeters trigger primitive generator (TPG) will stream single crystal data from the on-detector to the backend electronics, in contrast to the lower-granularity output of the Phase-1 ECAL TPG that is restricted to providing trigger tower sums of 5×5 crystals. A schematic representation of the geometry of the ECAL barrel in the Regional Calorimeter Trigger (RCT) is shown in Fig. 3. The barrel is spanned by 36 RCT cards, each spanning 17×4 towers in $\eta \times \phi$. Each RCT card is subdivided into five “regions” as shown in Fig. 4. After initial clustering and processing, the outputs of the RCT card are sent to the Global Calorimeter (GCT) trigger, which is processed in three cards as shown in Fig. 5.

1.3.2 Phase-2 electron/photon reconstruction algorithm

The standalone barrel algorithm for reconstructing and identifying electrons and photons in the Phase-2 Level-1 Trigger takes as input the digitized response of each crystal of the barrel ECAL, with a



Figure 2: Summary of the links between the trigger primitives (*first column*), the trigger objects (*second column*), the Level-1 algorithms used in the menu (*3rd column*), and the physics channels (*4th column*), from [CITE] <https://cds.cern.ch/record/2714892/files/CMS-TDR-021.pdf>, where a full description of the Phase-2 L1 algorithms can be found. This work focuses on developments for the Standalone Calorimeter electron and photon (“EG”) reconstruction algorithm.

granularity 0.0175×0.0175 in $\eta \times \phi$, which is 25 times higher than the input to the Phase-1 trigger, which consisted of trigger towers with a granularity of 0.0875×0.0875 . In HCAL the tower size of 0.0875×0.0875 is unchanged. The trigger algorithm is designed to closely reproduce the algorithm used in the offline reconstruction, with limitations and simplifications due to trigger latency.

In the RCT, an initial requirement of $p_T > 0.5$ GeV is imposed on the input trigger primitives (i.e. energies from the ECAL crystals and HCAL towers) to reject contribution from pileup. In one of the regions inside a RCT card (Fig. 4), the crystal containing the highest energy deposit is identified as the seed crystal, as shown in Fig. 6. The energy in the crystals in a window of size 3×5 in $\eta \times \phi$ around the seed cluster is added into a cluster. The energy is considered “clustered”. The process is repeated with the remaining “unclustered” energy, until up to four clusters are produced in the region.

To improve e/γ identification and to reduce background contributions, identification and reconstruction algorithms are implemented at this stage:

- Shower shape: The energy deposit sums around the seed crystal is computed in windows of size 2×5 and 5×5 (Fig. 6, *dashed lines*), with true e/γ clusters tending to produce showers that deposit most of their energy in a 2×5 region.
- Bremsstrahlung recovery: e/γ tend to spread in the ϕ direction due to charged particles being bent by the magnetic field of the CMS solenoid. If sufficient energy comparable to the core 3×5 cluster is found in the adjacent 3×5 windows (Fig. 6, *shaded yellow*), the energy is added to the core cluster and no longer considered unclustered energy.

After parallel processing in the regions, the clusters in a RCT card are stitched together if they are located directly along the borders of a region (Fig. 3). The remaining unclustered ECAL energy is summed into ECAL towers.

From each RCT card, the twelve highest-energy clusters, as well as any remaining unclustered energy, are sent to the GCT. Since each GCT card has information from sixteen RCT cards (Fig. 5), final stitching across the boundaries of the RCT cards is performed. One more identification algorithm is performed at this stage:

- Isolation: One handle to reject backgrounds from e.g. pileup, comes from the tendency for background to be spread more uniformly across a large area in the detector, whereas genuine e/γ are expected to produce showers concentrated in the 3×5 crystal window. The energy sum in a large window of 7×7 in towers is computed and used to reject background.

The performance of the standalone barrel e/γ algorithm in Phase-2 conditions is summarized in the efficiency and rates. The efficiencies are measured with a simulated Monte Carlo sample containing electrons. The rates are measured with a simulated minimum bias sample intended to closely mimic generic proton-proton collisions in the CMS detector. The performance of the Phase-2 emulator discussed in this work, which closely mimics the firmware logic and uses fixed-precision integers, is shown to be comparable to the previous emulator which used floats and idealized logic.

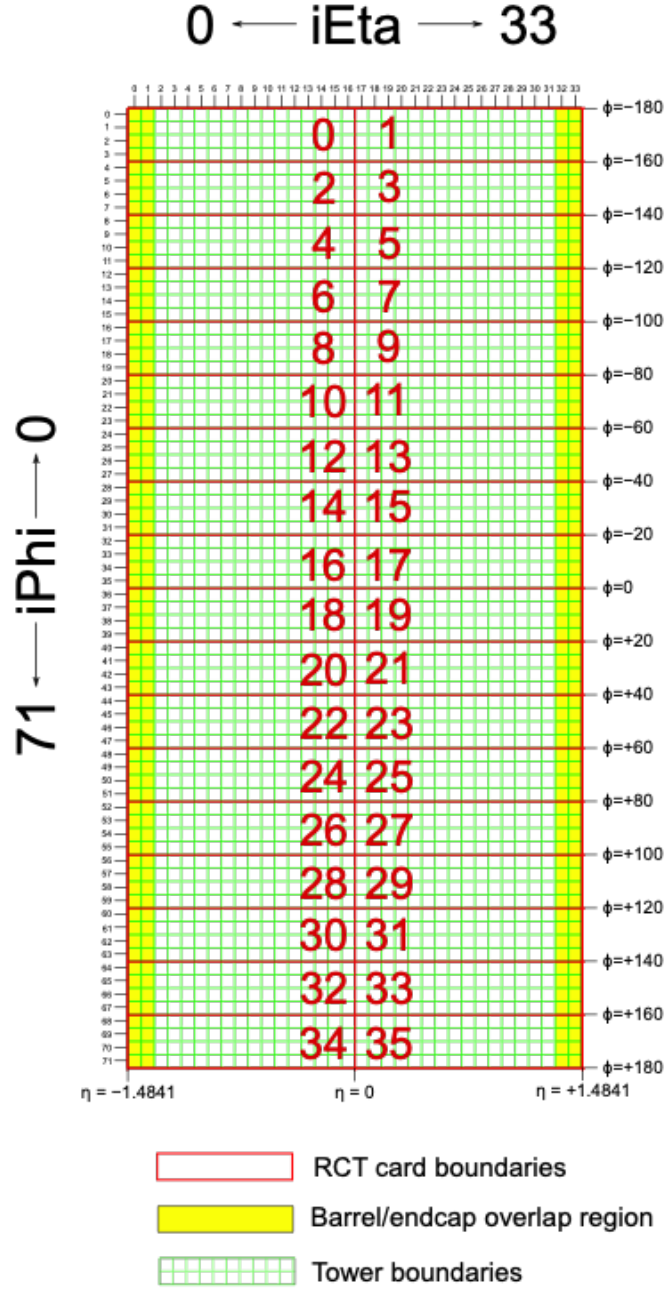


Figure 3: Schematic of the geometry of the Phase-2 ECAL barrel in the Regional Calorimeter Trigger (RCT), showing the division of the barrel region into 36 Regional Calorimeter Trigger (RCT) cards (*red*). Each card spans 17×4 towers in $\eta \times \phi$ (*green*), and each tower is 5×5 in single crystals in $\eta \times \phi$. Towers in the overlap region (*shaded yellow*) are read out to both the barrel and endcap.

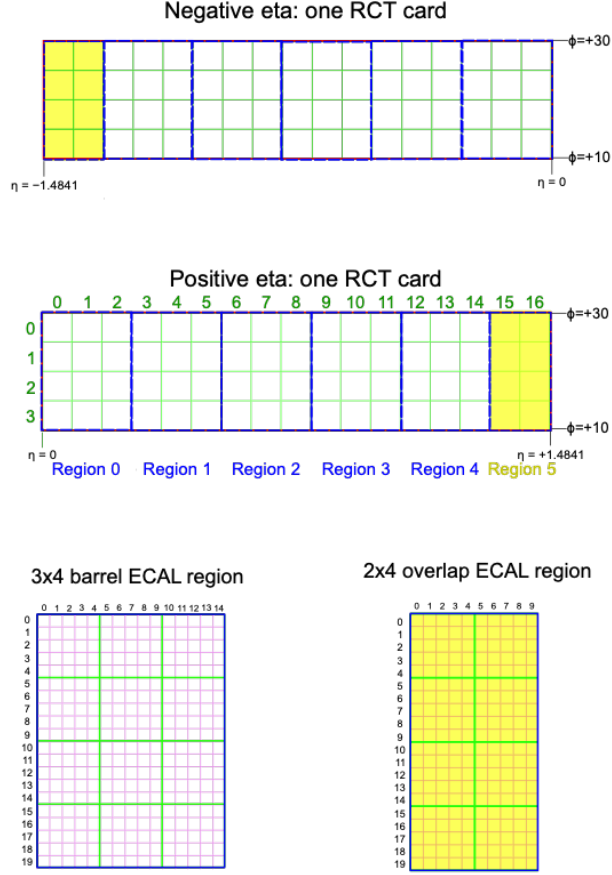


Figure 4: Schematic of two example RCT cards in the negative eta (*top*) and positive eta (*center*) regions of the ECAL barrel. Each RCT card is divided into five regions: four regions are of size 3×4 towers in $\eta \times \phi$ (*bottom left*), and a fifth smaller overlap region of size 2×4 towers (*bottom right*). Each tower is 5×5 ($\eta \times \phi$) in crystals.

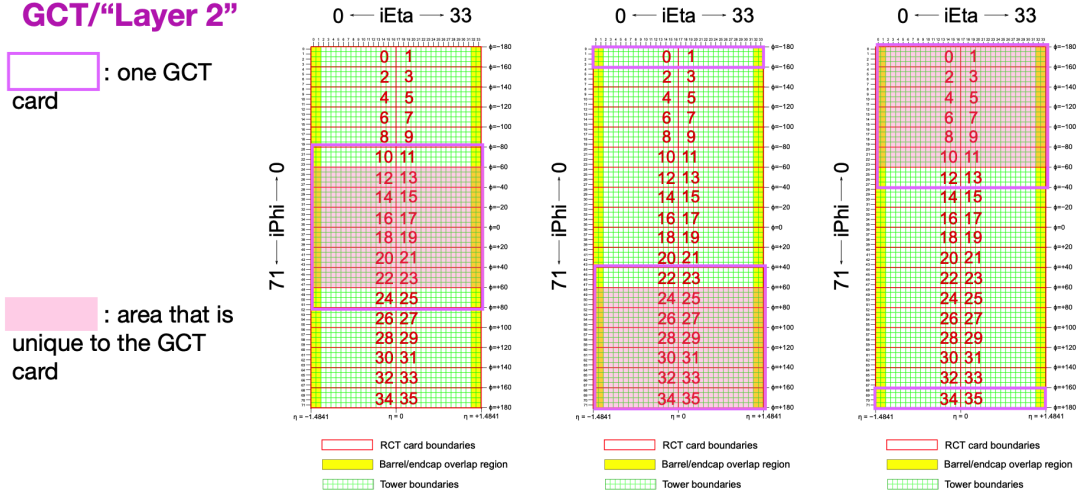


Figure 5: Schematic of the Phase-2 ECAL barrel in the Global Calorimeter Trigger (GCT), which will process the outputs of the Regional Calorimeter Trigger (RCT) in three cards (*magenta highlights*). Each card in the GCT processes the equivalent of sixteen RCT cards, with the center twelve being unique to that GCT card (*shaded pink*), and the remaining four processed in overlap with the other GCT cards.

3x4 barrel ECAL region

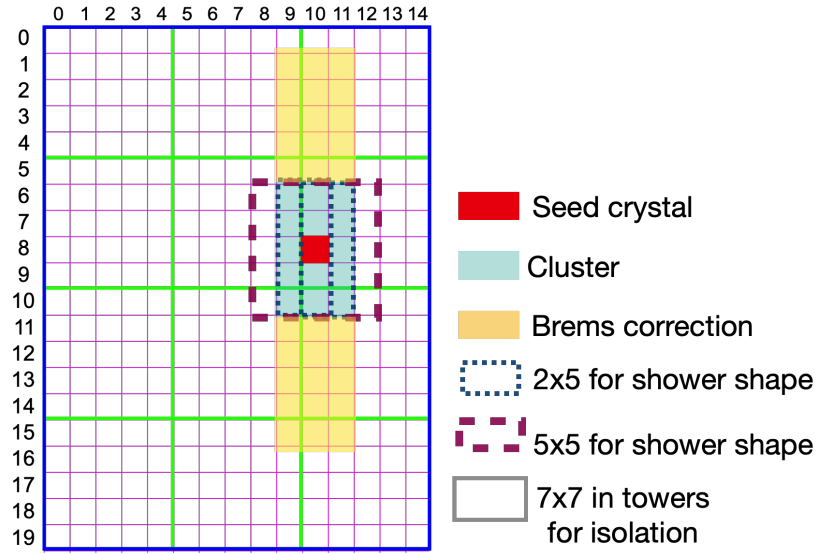


Figure 6: Illustration of an example electron/photon (e/γ) cluster in the Phase-2 Level-1 Trigger standalone barrel e/γ reconstruction, in a region of 15×20 crystals (3×4 towers). Each small pink square is one crystal, the highest-granularity ECAL trigger primitives available to the L1 Trigger in Phase-2. The core cluster consists of the energy sum in a 3×5 window of crystals, (*shaded light blue*) centered around the seed crystal (*red*). Bremsstrahlung corrections are checked in the adjacent 3×5 windows in the ϕ direction (*shaded light yellow*). The relative energies in windows of size 2×5 and 5×5 in crystals (*dashed dark blue and dark red*) are used to compute shower shape variables to identify true e/γ objects. Lastly, an isolation sum is computed in a window of size 7×7 in towers (not shown in figure).

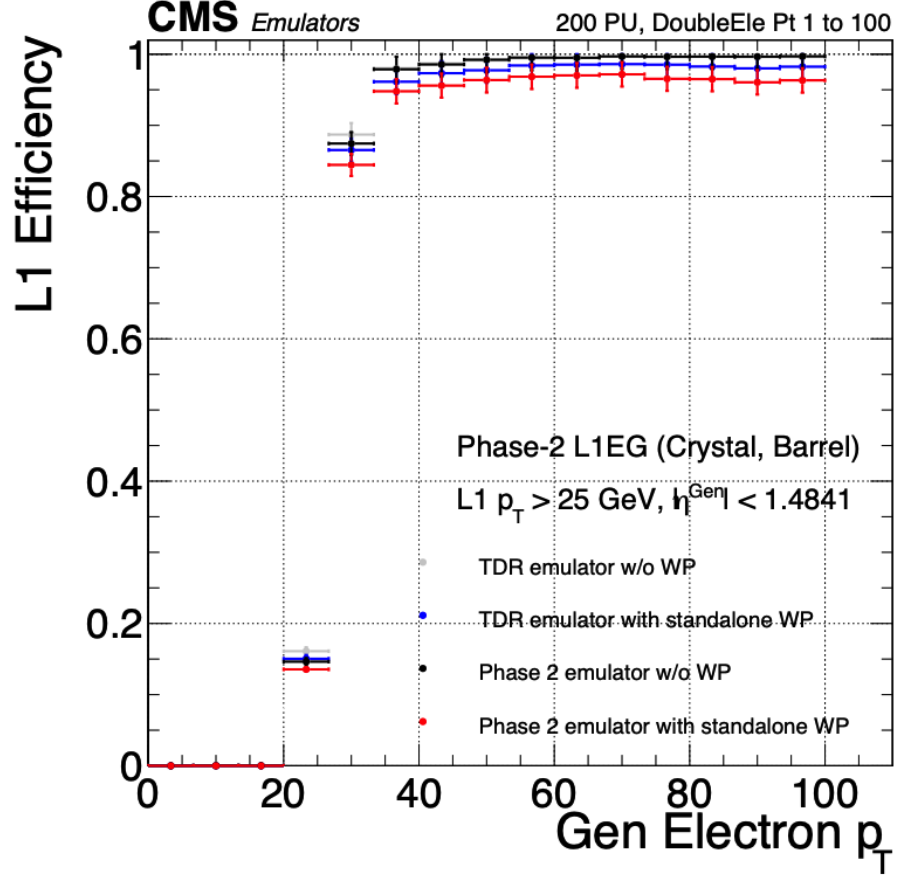


Figure 7: Efficiency of the standalone barrel e/γ reconstruction, measured in a simulated sample of electrons, as a function of the true electron’s transverse momentum p_T . The performance of the previous, idealized algorithm as shown in the 2021 TDR [CITE] with and without the isolation and shower shape discrimination variables (“standalone working point/ WP”) (dark blue, grey). The Phase-2 emulator discussed in this work with and without the same working point (black, red) is shown to have comparable performance.

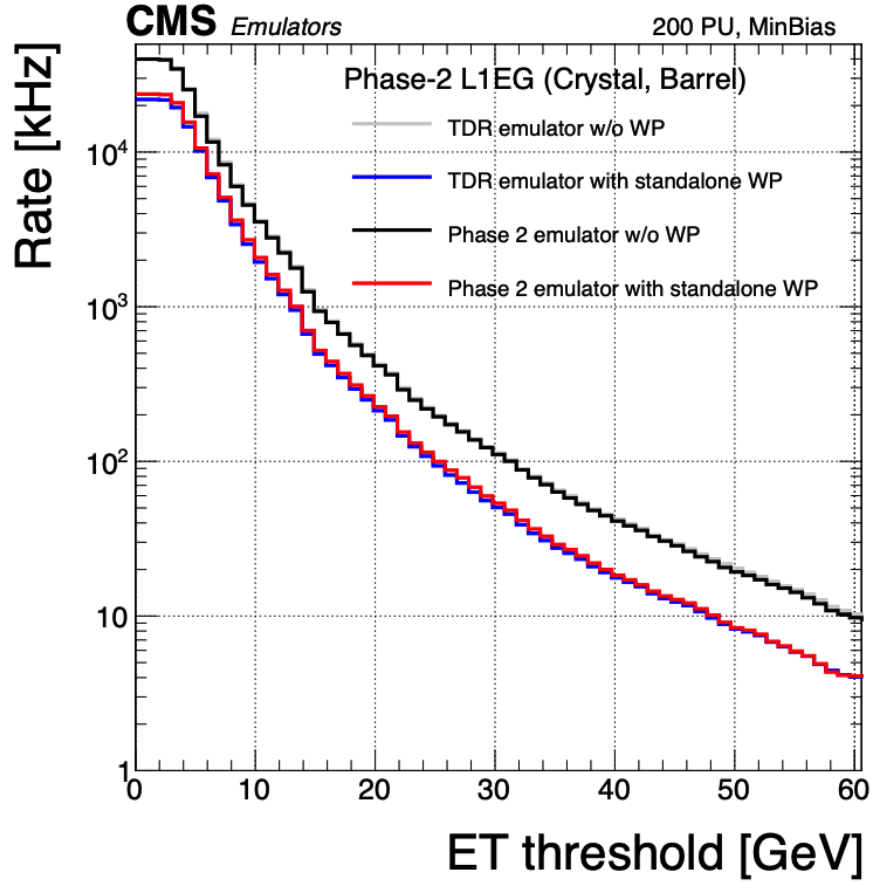


Figure 8: Rates of the standalone barrel e/γ reconstruction, evaluated on a minimum bias sample, measured as a function of the minimum energy (E_T) required of the reconstructed e/γ object in each event. The performance of the previous, idealized algorithm as shown in the 2021 TDR [CITE] with and without the isolation and shower shape discrimination variables (“standalone working point/ WP”) (*dark blue, grey*). The Phase-2 emulator discussed in this work with and without the same working point (*black, red*) is shown to have comparable performance.